

PARTIAL ACCRETION IN THE PROPELLER STAGE OF LOW MASS X-RAY BINARY AQL X-1

C. GÜNGÖR,^{1,2} K. Y. EKŞİ,¹ E. GÖĞÜŞ,² AND T. GÜVER³

¹*İstanbul Technical University, Faculty of Science and Letters, Physics Engineering Department, 34469, İstanbul, Turkey*

²*Sabancı University, Faculty of Engineering and Natural Science, Orhanlı – Tuzla, 34956, İstanbul, Turkey*

³*İstanbul University, Science Faculty, Department of Astronomy and Space Sciences, Beyazıt, 34119, İstanbul, Turkey*

(Received —, 2017; Revised —, 2017; Accepted February 28, 2022)

ABSTRACT

Aql X-1 is one of the most prolific low mass X-ray binary transients (LMXBTs) showing outbursts almost annually. We present the results of our spectral analyses of RXTE/PCA observations of the 2000 and the 2011 outbursts. We investigate the spectral changes related to the changing disk-magnetosphere interaction modes of Aql X-1. The X-ray light curves of the outbursts of LMXBTs typically show phases of fast rise and exponential decay. The decay phase shows a “knee” where the flux goes from the slow decay to the rapid decay stage. We assume that the rapid decay corresponds to a weak propeller stage at which a fraction of the inflowing matter in the disk accretes onto the star. We introduce a novel method for inferring, from the light curve, the fraction of the inflowing matter in the disk that accretes onto the NS depending on the fastness parameter. We determine the fastness parameter range within which the transition from the accretion to the partial propeller stage is realized. This fastness parameter range is a measure of the scale-height of the disk in units of the inner disk radius. We applied the method to a sample of outbursts of Aql X-1 with different maximum flux and duration times. We show that different outbursts with different maximum luminosity and duration follow a similar path in the parameter space of accreted/inflowing mass flux fraction versus fastness parameter.

Keywords: accretion, accretion disks — stars: neutron — X-rays: binaries — X-rays: individual
(Aql X-1)

arXiv:1709.02378v1 [astro-ph.HE] 7 Sep 2017

1. INTRODUCTION

Low mass X-ray binaries (LMXBs) are systems containing an accreting compact object—a neutron star (NS) or a black hole—and a low mass companion ($M_c \lesssim 1 M_\odot$). In these systems, the mass transfer mechanism is the Roche lobe overflow (Frank et al. 2002). The transferred matter has angular momentum and forms an accretion disk rather than directly infalling onto the compact object (Pringle & Rees 1972). Matter in the bulk of the disk rotates in Keplerian orbits and slowly diffuses inwards while the angular momentum is transported outwards by turbulent viscous processes (Shakura & Sunyaev 1973).

If the accreting object is a NS the inner parts of the disk may be disrupted at a location beyond the stellar surface. The location of the inner radius of the disk, R_{in} , is determined by the balance between the material and magnetic stresses in the disk (Ghosh & Lamb 1979a,b) which in turn depend on the mass inflow rate \dot{M} in the disk, the magnetic dipole moment μ_* and the spin angular velocity Ω_* of the star (Lamb et al. 1973). Such magnetized star-disk systems (see Romanova & Owocki 2015, for a review) may show three different stages depending on the relation between the inner radius of the disk and the two other characteristic radii; the corotation radius $R_c = (GM_*/\Omega_*^2)^{1/3}$ and the radius of the light cylinder $R_L = c/\Omega_*$ (Lipunov et al. 1992) where G is the gravitational constant, c is the speed of light and M_* is the mass of the star:

- The *accretion* stage in which $R_{\text{in}} < R_c$ resulting with most (if not all) of the mass flux in the disk to reach to the surface of the NS.
- The *propeller* stage (Illarionov & Sunyaev 1975) in which $R_c < R_{\text{in}} \lesssim R_L$ resulting with none (if not a small fraction) of the inflowing mass to reach the surface of the NS due to centrifugal barrier formed by the rapidly rotating magnetosphere.
- The *radio pulsar* stage in which R_{in} is even further away from the star, possibly larger than R_L .

The gravitational potential energy of infalling material powers the X-ray luminosity:

$$L_X = GM_*\dot{M}_*/R_* \quad (1)$$

(Davidson & Ostriker 1973) where R_* is the radius of the NS. Here \dot{M}_* is the mass accretion rate onto the NS and this may be different than the mass flow rate in the disk, \dot{M} , in unsteady regime such as occurring during an outburst.

Accreting millisecond X-ray pulsars (AMXPs) (Wijnands & van der Klis 1998) constitute a subclass of

LMXB systems which show coherent pulsations in their X-ray light curves resulting from accretion onto the magnetic pole of a NS from a disk truncated by magnetic stresses (see Patruno & Watts 2012, for a review). All AMXPs are transient systems showing outbursts in their X-ray light curves. A typical X-ray light curve of an outburst displays a fast rise and an exponential decay. Following the released energy during an outburst, spectral state transition is realized from the low-hard state (lower luminosity, harder spectrum) to the high-soft state (higher luminosity, softer spectrum) and vice-versa. In the hard state the spectrum outweighed by hard/Comptonized with a soft/thermal component and in the soft state the spectrum is more dominated by soft/thermal component Lin et al. (2007). Accordingly, \dot{M} rises steeply and declines slowly during the outburst within several weeks while magnetic dipole moment and angular velocity of the neutron star are relatively constant. As \dot{M} changes these systems may manifest the above mentioned stages of disk-magnetosphere interaction. AMXPs may thus serve as a lab for exploring the transitions between these different stages.

The decay stage of the X-ray light curves of AMXPs show a ‘knee’ marking the transition from a slow decline to a rapid decline stage (e.g. Ibragimov & Poutanen 2009). The cause of this change in their light curve was suggested to be a transition from the accretion stage to the propeller stage (Zhang et al. 1998a; Gilfanov et al. 1998; Campana et al. 1998; Asai et al. 2013) as assumed in this work. Similar ‘knees’ in the light curves are seen in black hole binaries which do not have magnetic fields and can not show propeller effect. Such transitions are assumed in some other references to be due to thermal disk instability model (see Lasota 2001, for a review). The pulsations of SAX J1808.4-3658 are detected even at very low luminosities at which the system would be expected to be well in the propeller stage (Menou et al. 1999; Ustyugova et al. 2006; Romanova et al. 2004). This may indicate that the “propeller effect” is not ideal but a fraction

$$f \equiv \dot{M}_*/\dot{M} \quad (2)$$

of the inflowing mass reaches the surface of the star (Asai et al. 2013; Campana et al. 2001; Cui 1997). This fraction would be a function of the fastness parameter of the system

$$\omega_* \equiv \Omega_*/\Omega_K(R_{\text{in}}) = (R_{\text{in}}/R_c)^{3/2} \quad (3)$$

(Elsner & Lamb 1977) where $\Omega_K = \sqrt{GM/R^3}$ is the Keplerian angular velocity in the disk. In the simplest picture of an ideal propeller surrounded by an infinitely

thin disk, f is a step function

$$f(\omega_*) = \begin{cases} 1, & \text{for } \omega_* \leq 1 \\ 0, & \text{for } \omega_* > 1 \end{cases} \quad \text{ideal propeller.} \quad (4)$$

In real disks with a finite scale-height, H , a regime of partial accretion may be realized in which f is expected to change smoothly with ω_* . This is because accretion can proceed from higher latitudes of the disk even while the disk midplane is propelled (Romanova et al. 2004; Ekşi & Kutlu 2011). Indeed, the disk may become thicker to allow for such accretion as the fastness parameter goes above unity, or transition to the propeller stage may be induced as a result of the evaporation and thickening of the inner disk (Güngör et al. 2014). The smoothness of the transition will be a measure of $H(R_{\text{in}})/R_{\text{in}}$. Being a dimensionless function of a dimensionless parameter $f = f(\omega_*)$ should be unique for different outbursts of a system. In general f may also depend on the inclination angle between the rotation and magnetic axis and so may vary for different systems. Theoretical estimates for $f(\omega_*)$ were presented by Lipunov & Shakura (1976) for spherical accretion and by Menou et al. (1999) for the quasi-spherical disk accretion case. The latter authors showed that $f = (3/8)\omega_*^{-4}$ at the $\omega_* \gg 1$ limit. The general case was investigated by Ekşi & Kutlu (2011) with an application to SAX J1808.4–3658, another AMXPs. In the present work we attempt to extract $f = f(\omega_*)$ from observations, for the first time in literature as to our knowledge.

Aql X-1 is one of the most active LMXBTs, exhibiting about 25 outbursts from 1996 until 2016 (Güngör et al. 2017; Meshcheryakov et al. 2017; Maitra & Bailyn 2008; Campana et al. 2013; Asai et al. 2013). Over 20 years of observations of Aql X-1, the pulsations were observed only in a very short duration of 150 s which makes the source is classified as an intermittent AMXP. The observed spin frequency of $\nu_* = 550.27$ Hz (Casella et al. 2008) and the observations of Type-I X-ray bursts (Koyama et al. 1981) firmly establish that the compact object in this system is a neutron star.

In this work we investigate the Rossi X-ray timing explorer/proportional counter array (RXTE/PCA) observations of Aql X-1, to study the transition into and from the accretion regime to the propeller regime with the assumption of that the outbursts of Aql X-1 happen as a result of viscous thermal instability. In section 2, we explain the details of data reduction procedures, and present their outcomes. In section 3, we present the method we use to infer $f(\omega_*)$ from the X-ray light curves. In section 4, we apply the method to the outcomes of our observational analysis and present

the results. Finally, in section 5, we discuss our results and conclude.

2. OBSERVATION AND DATA ANALYSIS

The detected X-ray luminosity is assumed to originate from the NS surface and the inner parts of the disk. In order to separate these two components we performed a spectral analysis of RXTE/PCA observations for the 2000 and 2011 outbursts (52 and 51 pointed observations, respectively). We eliminated observations with thermonuclear bursts and those with very low S/N ratio. The average exposure times of the selected observations ~ 1800 s and ~ 1450 s, respectively. These observations cover the entire durations of both outbursts, i.e., the fast rising, the slow decay and the fast decay phases.

We analysed the RXTE/PCA data using HEASOFT¹ version 6.17. Since Aql X-1 is a very bright source in the X-ray band, we used only PCU2 (proportional counter unit) which was always operational in all pointings. We generated the response files for each observation using PCARSP version 11.7.1 and we used the latest module file² for the background model.

All spectra were modelled in the 3.0 – 30.0 keV range using XSPEC package³. We added a 1.0% systematic error to the data during chi-squared test to take into account systematic instrumental uncertainties. We hypothesize two different models to represent the spectrum. We first modelled all spectra using a combination of blackbody, disk blackbody and a Gaussian component to account for fluorescent iron emission. Second, we take the Comptonization into account with the assumption of that the NS surface and the Comptonization cloud have the same temperature.

2.1. Model I: Blackbody assumption

The blackbody component (*body* in XSPEC) represents the X-ray emission originating from the hot spot at the pole of the NS fed by accretion. The disk blackbody component (*diskbb* in XSPEC) represents the X-ray contribution of the inner layers of the accretion disk. After determining the best fit parameters for *blackbody + disk blackbody* model for the RXTE/PCA data, a Gaussian line is added to represent the iron line. We used a constant neutral hydrogen column density of $N_{\text{H}} = 3.4 \times 10^{21}$ atoms cm^{-2} (Maccarone & Coppi 2003) using the model by Balucinska-Church & McCammon (1992, *phabs* in XSPEC). In Figure 1, we show

¹ <https://heasarc.gsfc.nasa.gov/docs/software/lheasoft/>

² [pca_bkgd_cmbrightvle_eMv20051128.mdl](https://heasarc.gsfc.nasa.gov/docs/software/lheasoft/pca_bkgd_cmbrightvle_eMv20051128.mdl)

³ An X-Ray Spectral Fitting Package v12.8.2, <https://heasarc.gsfc.nasa.gov/xanadu/xspec/>

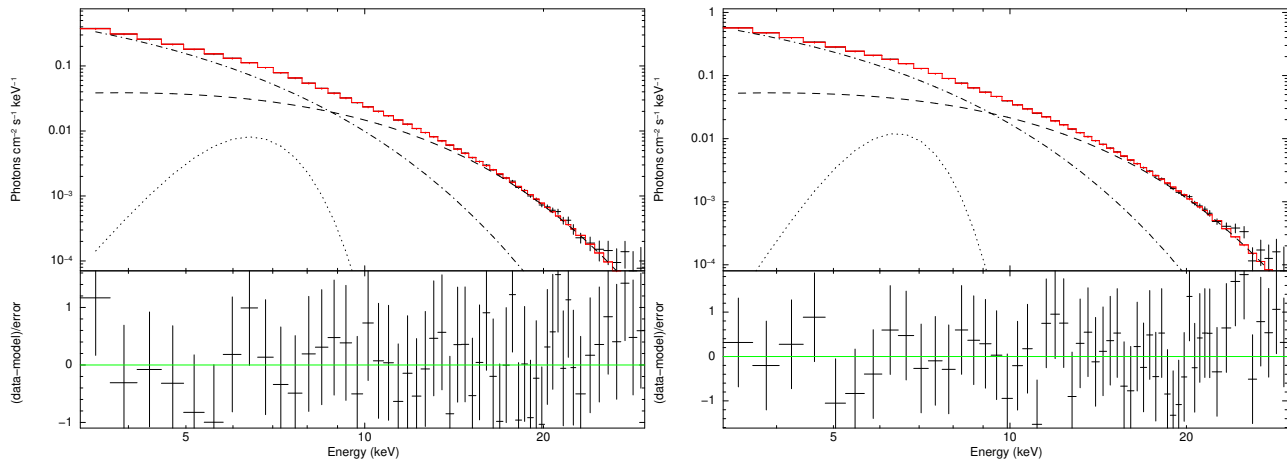


Figure 1. The X-ray spectrum of Aql X-1 during outburst obtained by RXTE/PCA in the 3.0 – 30.0 keV energy range during the 2000 (ObsID 50049-02-08-03, *the left panel*) and the 2011 (Obs ID 96440-01-05-01, *the right panel*) outbursts, respectively. The best fits obtained by using the $bb+diskbb+(ga)$ model are shown with red line. Lower panels show the residuals in terms of sigma. The dashed, the dashed dotted and the dotted curves show the blackbody, disk blackbody and the Gaussian components, respectively.

an example of the fits we performed for each data set. A typical normalisation value of diskbb component is around $(R_{\text{in}}/D_{10})^2 \cos \theta = 100$ (for ObsID 50049-02-08-03) where R_{in} is the inner radius of the disk in km, D_{10} is the distance in units of 10 kpc and θ is the viewing angle of the disk, giving $R_{\text{in}} = 4.5 \text{ km}/\sqrt{\cos \theta}$ assuming the source is at 4.5 kpc (Galloway et al. 2008). This value of R_{in} is smaller than typical radius of a NS for a face-on disk ($\theta = 0$) and reaches reasonable values for $\theta \gtrsim 75^\circ$ corresponding to almost edge on view. The reason for small inner radius may also be an indication that Comptonization is significant (Lin et al. 2007) and the components are not fully separated as we assume.

We calculated the unabsorbed fluxes for the best fit of the X-ray spectra using *blackbody + disk blackbody + Gaussian* model for the blackbody and the disk blackbody components, separately in the range of 3.0 – 30.0 keV (F_{3-30}) for RXTE/PCA data. Bottom left and bottom right panels of Figure 2 and Figure 3 show the light curves for each component for the 2000, the 2011 outburst, respectively.

Moreover, by taking the *pivot* energy (E_{pivot})—the energy in which we used to calculate hardness parameter—as 10 keV, we computed the fluxes for 3.0 – 10.0 keV (F_{3-10}) and 10.0 – 30.0 keV (F_{10-30}) energy ranges, following Zhang et al. (1998a). We then obtained the hardness evolution using the ratio of F_{10-30}/F_{3-10} (Figure 2 and Figure 3 middle left, middle right). The free parameters of the blackbody and the disk blackbody are the temperature of the blackbody component (T_{bb}), the inner disk temperature of the disk blackbody component ($T_{\text{diskbb}}(R_{\text{in}})$) and the normalisations of the models. We show the evolution of T_{bb} (top left) and $T_{\text{diskbb}}(R_{\text{in}})$ (top

right) in keV in upper panels of Figure 2 and Figure 3. We provide the final model parameters in Table 2 and Table 3 for the 2000 and 2011, respectively.

In both components, we see that the spectral parameters evolve in a similar way. With the commence of the outburst T_{bb} drops down to ~ 2 keV while hardness ratio of the blackbody decreases to ~ 1 and both parameters stay stable during the bright phase of the outburst. It must be mentioned that in the low-hard state, the temperatures throughout the model I are very high in which this shows the lack of the model I in low-hard state. The hardness decreases to the pre-outburst level before the outburst ends and the system passes to the quiescent stage. This transition to the rapid-decay stage, rather than to the quiescent stage, marks the transition to the hard state from the soft state (see Remillard & McClintock 2006, for a BH study which is applicable to NSs).

Zhang et al. (1998b) argued that the transition in the hardness ratio is caused by the *propeller effect* (Illarionov & Sunyaev 1975). These critical moments are used to identify the beginning and the terminal of slow decay stage which are also used as the fit range in our method described in section 3.

2.2. Model II; Comptonised blackbody assumption

Even though the blackbody assumption works in many cases, the upscattering of the photons by the coronal electrons must also be taken into account. We checked the role of Comptonization by modelling all spectra in the low-hard state and few examples in the high-soft state corresponding to accretion using a similar combination as in model I by adding a Comptonization model (*comptTT* in XSPEC, Titarchuk &

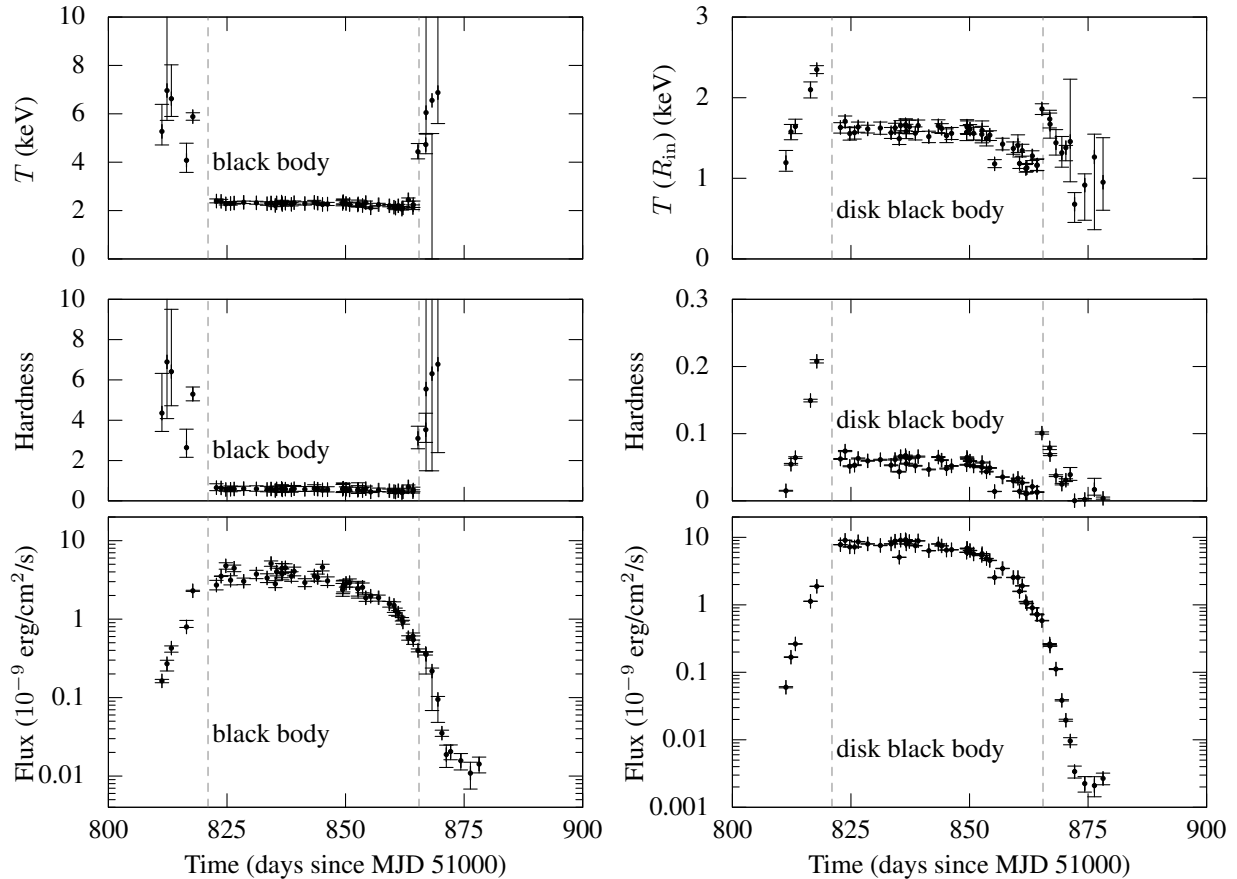


Figure 2. Evolution of spectral parameters during the 2000 outburst of Aql X-1. The top panels show the time evolution of the blackbody temperature (left) and the inner disk temperature of the blackbody (right). The middle panels show the time evolution of the hardness parameter only for the blackbody component (left) and only for disk blackbody component (right). The bottom panels show the evolution of the flux of the blackbody component (left), and the disk blackbody component (right). The vertical lines show the times of the state transitions.

Lyubarskij 1995) in which the Wien temperature of the Comptonization model is linked to the temperature of the blackbody model under the assumption that photons from the NS surface act as the seed for inverse Compton process. As it is mentioned in Titarchuk (1994), plasma temperature is connected to the optical depth and fairly constrained. Thus, plasma temperature is set to a reasonable value, 15.0 keV (Lin et al. 2007).

The geometry is chosen as disk and the β parameter of Comptonization is obtained from the optical depth (τ) using analytic approximation (see Titarchuk & Lyubarskij 1995, for details). τ and the normalisation of the Comptonization model are free fit parameters. For the X-ray contribution of the heated inner disk layers, we added the disk blackbody component just as in model I. We added the Gaussian emission line component with the peak energy of 6.4 keV and maximum sigma of 1.0 keV to account for Fe line emission. The input parameters of the disk blackbody component to the fit are taken from the resulting fit of model I to better

constrain the Comptonization effect on the blackbody component and to check whether adding Comptonization corrects the high blackbody temperatures in the low-hard state.

We provide resulting parameters of model II analysis in Table 4 and Table 5 for the 2000 and the 2011 outbursts, respectively. Model II is preferable to model I for representing the T_{bb} better in the fast rising phase of the X-ray light curve which corresponds to low-hard state since model I gives T_{bb} values unphysically high. We tracked the time evolution of τ during outburst. τ drops down to the zero level, following the trend of hardness, indicating that the system changes from low-hard state to high-soft state. The variance of the parameters τ and hardness of the blackbody component implies that Comptonization becomes ineffective in the high-soft state. It is possible to interpret this simply by suggesting that the contribution of Comptonization during the accretion becomes harder to determine when the disk is closer the star and has enhanced contribu-

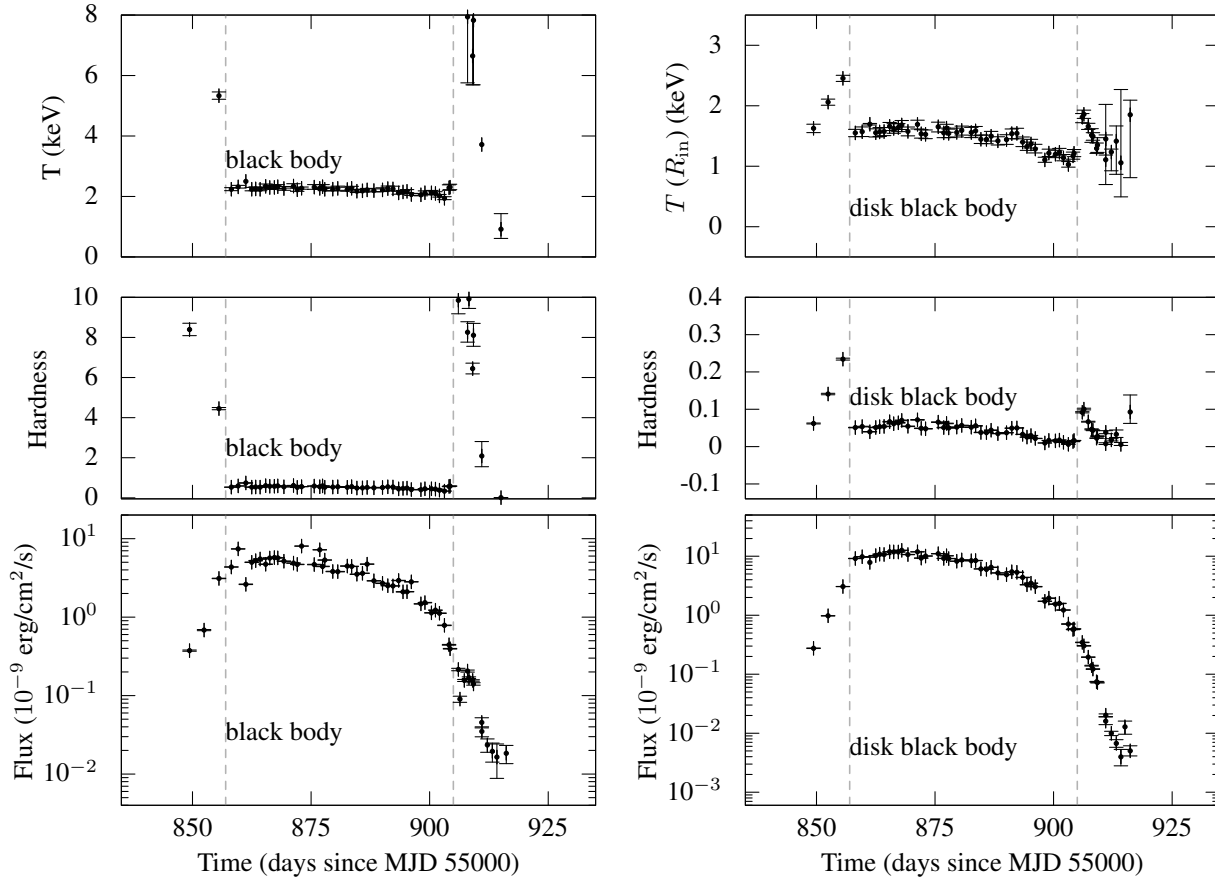


Figure 3. Same as [Figure 2](#) but for the RXTE/PCA data during the 2011 outburst of Aql X-1.

tion to the total X-ray flux. The result implies that the blackbody component is sufficient for representing the soft-high. We will then assume that the light curve of the blackbody component represents the time evolution of the luminosity of accretion onto the NS surface.

3. THE PARTIAL ACCRETION REGIME OF OUTBURSTS

Here, we propose a simple method for extracting $f(\omega_*)$ from the light curve, $L_X(t)$. The method is based on the following assumptions:

- The rapid decay stage is a consequence of transition of the system to the propeller stage $\omega_* > 1$ and is not due to irradiation or any other process.
- The transition to the propeller stage occurs because material stress declines with the accretion rate hence is balanced by the magnetic stresses at a larger distance, now further away from the corotation radius. We note here that BH systems also may have receding inner disk radii possibly as a result of disk evaporation (see e.g. [Liu et al. 1999](#); [Meyer et al. 2000](#)). If the same mechanism also

works in NS systems a different analysis than ours has to be employed.

- The decay of the mass inflow rate \dot{M} continues its evolution with no modification upon the transition of the system from accretion to the propeller stage though a smaller fraction of it can now accrete onto the star leading to the appearance of rapid decline. This is possibly because of the delay in transferring the information of the changed inner boundary condition to the outer parts of the disk which keep transporting matter in.
- The angular velocity Ω_* and magnetic moment μ_* of the neutron star does not change significantly during an outburst.

We also assume $f = 1$ (meaning that $\dot{M}_* = \dot{M}$) in the slow decay stage before the knee though there is reason to believe that some of the matter donored by the companion is ejected from the disk by winds on the way to the innermost disk. Soon after the maximum is reached the disk establishes a quasi-equilibrium stage which evolves self-similarly ([Lyubarskij & Shakura 1987](#); [Lipunova & Shakura 2002](#); [Suleimanov et al. 2008](#))

where the mass flux will evolve as:

$$\dot{M}(t) = \dot{M}_0 \left(1 + \frac{t - t_0}{t_\nu}\right)^{-\alpha}. \quad (5)$$

Here t_ν is the time-scale of the outburst decay (viscous timescale) and \dot{M}_0 is the mass flux at t_0 which is the moment power-law decline starts. In the full accretion regime ($f = 1$) the luminosity follows this trend so that we can fix $\dot{M}_0 = L_0 R_* / GM_*$ where L_0 is the luminosity at the moment of t_0 . The value of the power-law index α depends on the pressure and opacity prevailing in the disk (Cannizzo et al. 1990; Ekşi & Kutlu 2011). We have fixed $\alpha = 1.25$ appropriate for a gas pressure dominated disk with bound-free opacity (Cannizzo et al. 1990). Although the inner parts of the disk for high accretion rates will be dominated by radiation pressure and electron scattering opacity, the mass flux throughout the disk is regulated by the outer parts where gas-pressure and bound-free opacity dominates.

Aql X-1 is a $\nu_* = \Omega_*/2\pi = 550.27$ Hz AMXP (Casella et al. 2008). The corotation and the light cylinder radii for a neutron star with this the spin frequency are $R_c = (GM_*/\Omega_*^2)^{1/3} = 2.5 \times 10^6$ cm (for $M_* = 1.4 M_\odot$) and $R_L = c/\Omega_* = 8.7 \times 10^6$ cm, respectively. The maximum critical fastness parameter above which the inner radius goes beyond the light cylinder for this system is $\omega_{* \max} = (R_L/R_c)^{3/2} \simeq 6.5$.

The inner radius of the disk is proportional to the Alfvén radius, $R_{\text{in}} = \xi R_A$, where ξ is a constant of order unity and generally taken as $\xi = 0.5$ (Ghosh & Lamb 1979a,b)). The Alfvén radius (Davidson & Ostriker 1973) is

$$R_A = \left(\frac{\mu^2}{\sqrt{2GM\dot{M}}}\right)^{2/7} \quad (6)$$

where μ is the magnetic dipole moment of the star. This designation could be valid only if it does not yield an inner radius smaller than the radius of the NS. The disk could extend to the surface of the star only at the peak of brightest outbursts. As the Alfvén radius scales with the mass flux as $R_A \propto \dot{M}^{-2/7}$ which then implies, by Equation 3, that $\omega_* \propto \dot{M}^{-3/7}$ or rather

$$\omega_* = (\dot{M}/\dot{M}_c)^{-3/7} \quad (7)$$

where \dot{M}_c is the mass inflow rate that would place the inner radius on the corotation radius and is related to L_c , critical luminosity at which partial accretion starts, as $\dot{M}_c = L_c R_* / GM_* f_c$ where f_c is the fraction of mass flux at this critical stage. This corresponds to the luminosity at which rapid decline commences. The inner radius of disk in the quiescent stage at which $\dot{M} = 0$

was formalized by Özsükan et al. (2014) in the context of a putative supernova debris disk around the Vela pulsar assumed to be in a strong propeller stage. In the decay stage that we consider here for Aql X-1 we have already assumed mass keeps inflowing even for $\omega_* > 1$ and the system is in a weak propeller regime so we find the scaling of the Alfvén radius appropriate.

In the propeller stage we assume that the mass inflow rate in the disk determining the inner radius continues with the same trend. Thus if all this inflowing matter could accrete we would have a luminosity continuing with the same trend of the accretion stage with no knee. The presence of the knee is assumed to be a consequence of partial accretion in the propeller stage: thus a fraction f of \dot{M} can accrete. The rest of the material may be ejected from the system completely via jets (Tudose et al. 2009). In order to describe this partial accretion we replace the fraction $f(\omega_*)$ given in Equation 4 for the ideal propeller with a smoothed step function that varies from unity to $f_{\text{min}} < 1$

$$f = \frac{1}{2} \left[1 + f_{\text{min}} + (1 - f_{\text{min}}) \tanh\left(\frac{\omega_c - \omega_*}{\delta}\right) \right] \quad (8)$$

where $\omega_c (= 1)$ is the critical fastness parameter at which the transition between accretion and propeller stages, and δ is a measure of the abruptness of this transition.

We first fit the region between the maximum of the light curve and the knee using Equation 5 to determine t_ν , L_0 , t_0 and t_{knee} . We then fit the light curves from the maximum of the outburst to the end of the data using $f(t) = f[\omega_*(t)]$ with the initial fit values. From the latter fit we obtained the values of f_{min} and δ which are the free fit parameters.

The above analysis assumes that the X-ray luminosity totally originates from accretion onto the NS. For weakly magnetized neutron stars, such as Aql X-1, the inner radius of the disk is close to the star and the inner disk may contribute to the X-ray luminosity. To obtain the luminosity due to accretion onto the star alone one needs to use spectral analysis (in section 2).

We note that there are diverging views of how the propeller stage is realized. D'Angelo & Spruit (2010) argued that propeller stage at low accretion rates will be realized by accumulation of matter at the inner disk rather than being ejected out of the system. This will lead to bursts of enhanced accretion (Spruit & Taam 1993; D'Angelo & Spruit 2011) and steady state quiescent (dead) disk solutions (Sunyaev & Shakura 1977). The timescales for the bursts is the viscous time-scale at the inner disk ($\tau_\nu \sim 1$ ms) which is not resolved in the data we employ in this work. Whether the matter

is ejected or is retained in the disk, the accretion rate onto the star and hence X-ray luminosity will decline and, therefore, from the point of view of the present work analysing the fraction of accreting matter onto the star depending on the fastness parameter remain to be relevant.

4. APPLICATIONS

A broad classification of the outbursts of Aql X-1 is presented by Güngör et al. (2014) based on the maximum flux and the duration of the outbursts. Accordingly, Aql X-1 shows three main types of outbursts: (i) The *long-high* outbursts with outburst duration of 50 – 60 days and a maximum flux of 37 – 61 cnt/s. (ii) The *medium-low* outbursts with 40 – 50 days and a maximum flux of 13 – 25 cnt/s. (iii) The *short-low* outbursts with approximately 20 days duration time and reaching a maximum flux of 17 – 25 cnt/s.

As we focus on the energetic outbursts, after performing the spectral analysis to the RXTE/PCA data of the 2000 and the 2011 outbursts –both belonging to the long-high class– and obtaining the light curves only for blackbody components explained in subsection 2.1, we applied the procedure described in section 3 to calculate the fraction of mass flux reaching the NS in the propeller stage. In addition, to check the possible differences, we applied the technique to all-sky Monitor (ASM) data of the 2000 outburst, the monitor of all sky X-ray image (MAXI) data of the 2013 outburst and the most energetic one, 2016 outbursts (Güngör et al. 2017).

The decay stages of the 1997 and the 2010 outbursts of Aql X-1 have been studied by Campana et al. (1998) and Campana et al. (2014). In the latter work the authors concluded that the rapid decay stage is likely caused by the transition to the propeller stage. We, also, applied the method to these outbursts to investigate the mass transfer characteristic for different classes. In Figure 4, we show the light curves of all outbursts together with the fit function of Equation 5.

In Figure 5, we show $f \equiv \dot{M}_*/\dot{M}$ vs ω_* i.e. Equation 8 for all outbursts in our sample. The numerical values of the parameters f_{\min} and δ of Equation 8 and t_ν of Equation 5 obtained by fitting the lightcurve of each outburst (as described in § 3) are given in Table 1.

5. DISCUSSION

In this paper, we studied the evolution of the disk-magnetosphere interaction from accretion to the propeller regime using the X-ray data of Aql X-1.

We analysed the RXTE/PCA data of the 2000 and the 2011 outbursts of Aql X-1. We modelled each spectra using a combination of blackbody and disk blackbody

Table 1. Resulting values of the free parameters of the method.

	t_ν (days)	f_{\min} (10^{-3})	δ (10^{-2})
2000 RXTE	14.4	5.5	3.8
2011 RXTE	9.8	5.5 [†]	4.2
2000 ASM	8.0	29.8	2.3
2013 MAXI	45.5	30.0 [†]	4.3
2016 MAXI	17.6	10.3	3.7
1997 [‡]	7.3	0.8	3.6
2010 [‡]	17.1	0.5	3.7

[†]The values are fixed to the outcome of last outburst since there is no enough data to obtain base level of the step function.

[‡]The light curve data is taken from Campana et al. (2014).

and obtained the lightcurves and time evolution of the spectral parameters for each component separately.

The blackbody component represents seed photons released at the hot spot on the NS poles while Comptonization plays a role in the spectral formation. We checked the validity of the blackbody assumption using a Comptonization model (*comptT* in XSPEC, Titarchuk & Lyubarskij 1995) with a linked Wien temperature parameter to the blackbody temperature and showed that Comptonization is not significantly dominant during the slow decay stage. This supports the view of that X-ray flux due to accretion is represented by the blackbody radiation. Different models could be employed to separate the contributions of different components in the total X-ray flux (e.g. *nthcomp(blackbody)+diskbb*, Sakurai et al. 2012; Lin et al. 2007).

Although Comptonization is ineffective in the soft state, adding it to the model corrects the blackbody temperatures at the hard state. Temperatures inferred without employing Comptonization are too high to be explained via known physical processes (Obs # 1–5 in Table 2 and Obs # 1–3 in Table 3). The last two data of the hard state, however, show similarly high temperatures even with the Comptonization component included. These data correspond to the episode before the maximum of the X-ray light curve and the spectra at this episode is still hard while luminosity is high. This may indicate to a *high-hard interstage* which occurs at the rising stage of the outburst before the low-hard stage and high-soft stage at the decay stages. Considering that a similar situation exists in transitions from high-soft stage to low-hard stage, we suggest that the system shows a *pre-propeller* stage at the similar luminosity level while the disk drifts to the inner layers. As the

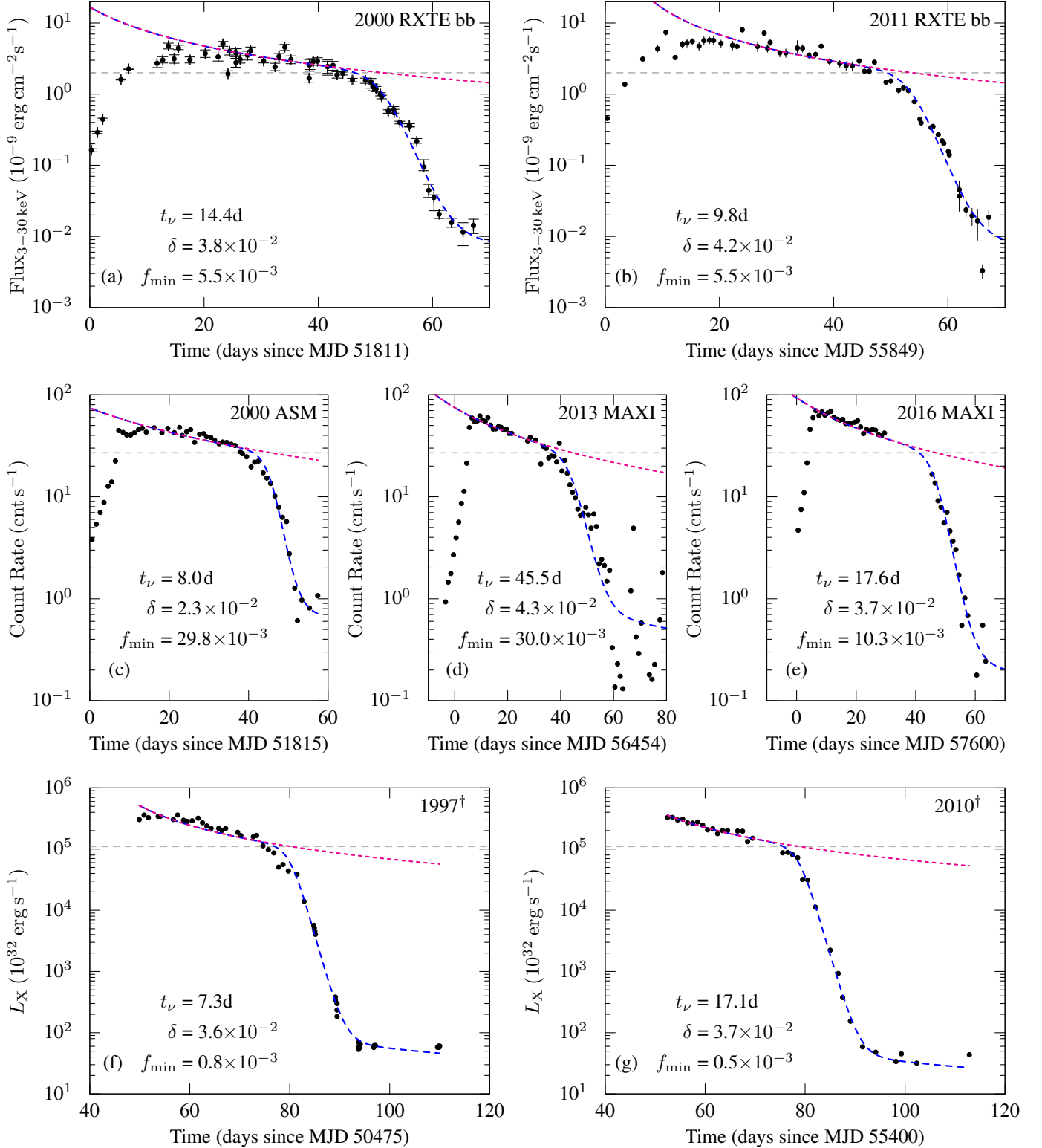


Figure 4. The X-ray light curves of the blackbody components of the RXTE/PCA data of the 2000 (a) and the 2011 (b) outbursts. The ASM light curve of the 2000 outburst (c). The MAXI light curves of the 2013 (d) and the 2016 (e) outbursts (Count rates are calibrated to ASM level). The horizontal lines show the L_c levels in Equation 5. The pink curves show the best fits of Equation 5 between maximum of outbursts and the knee. The blue curves show the best fits to the total data.

†The X-ray light curves of the 1997 (f) and the 2010 (g) outbursts obtained from Campana et al. (2014).

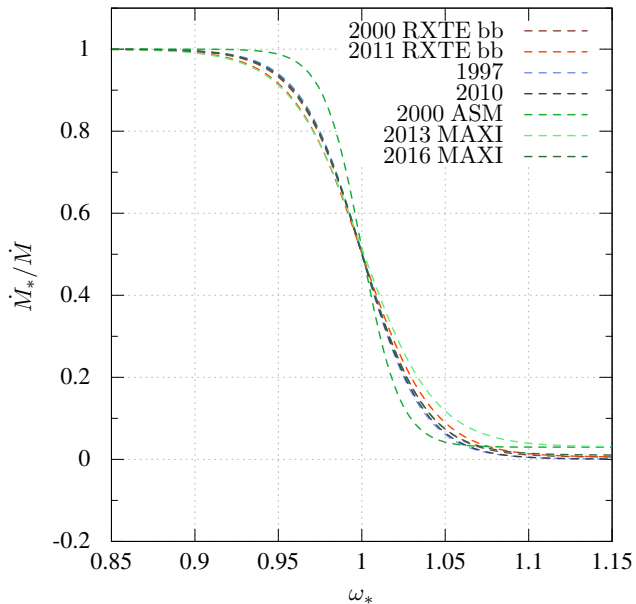


Figure 5. $f = \dot{M}_*/\dot{M}$ vs the fastness parameter ω_* relation obtained from the outbursts of Aql X-1.

rising phase of the X-ray light curve is shorter than the decay phase, the pre-propeller stage lasts shorter than the propeller stage.

Recently, (Tsygankov et al. 2017) suggested that the decline in X-ray flux during the outbursts of high mass X-ray binary systems (containing slowly rotating neutron stars) is due to transition to a cold (neutral; $T \lesssim 6500$ K) disk state. In this case, accretion rate is low due to the suppression of magnetorotational instabilities. In the case of Aql X-1, the rapid rotation and relatively small magnetic field of the compact object will likely eliminate the possibility of accretion from a cold disk (see Figure 3 of Tsygankov et al. 2017).

For probing the transitions from the accretion to the propeller stage, we introduced a novel method to determine the ratio of the mass accretion rate onto NS pole to the mass inflow rate at the inner disk, depending on the fastness parameter, from the observed X-ray light curve. The method depends on the assumptions that the rapid decay stage corresponds to the propeller stage at which partial accretion proceeds and that the X-ray flux is due to weak accretion onto the poles. Our results imply a more steeper decline of f with the fastness parameter than predicted by the existing theoretical models for spherical accretion (Lipunov & Shakura 1976) and quasi-spherical accretion (Menou et al. 1999).

Herein, the outcome of the analysis of the X-ray data of the 2000 and 2011 outbursts allows to better represent the emission from the hot spots on the NS as the result of accretion. By using only the blackbody light curves

for these outbursts, we transform the flux vs time data to the fraction ($f \equiv \dot{M}_*/\dot{M}$) vs fastness parameter (ω_*) domain. Comparing all outbursts in this domain find that different outbursts with different time scales and maximum fluxes follow a similar path in $f - \omega_*$. The step like function representing the outbursts in f vs ω_* space is a function constrained in a narrow band for this system (Aql X-1). The abruptness, δ , of the step function given in Equation 8 must be related to the thickness of inner layers of the disk (disk scale-height H) in units of inner disk radius, and the inclination angle between the rotation and magnetic dipole axis of the NS.

The transition to the propeller regime allows for an estimate of the magnetic field of the NS (Campana et al. 1998; Di Salvo & Burderi 2003; Asai et al. 2013; Campana et al. 2014; Mukherjee et al. 2015; King et al. 2016). Our continuous representation of the fraction of the accreting mass flux indicates that $f_c = 0.5$ (see Figure 5) when $R_{\text{in}} = R_c$ ($\omega_{\text{ast}} = 1$). This leads to an higher estimate of the magnetic dipole moment which is $\sqrt{2} \simeq 1.5$ times greater than the previous estimates which assume $f = 1$ when at this stage. We find that

$$\mu = 8.0 \times 10^{26} \text{ G cm}^3 M_{1.4}^{1/3} R_{10}^{1/2} \left(\frac{\xi}{0.5} \right)^{-7/4} \left(\frac{L_c}{1.1 \times 10^{37} \text{ erg s}^{-1}} \right)^{1/2} \quad (9)$$

where $M_{1.4}$ is the mass of the NS in units of 1.4 solar mass and $R_{10} = R_*/10^6$ cm. Here we assumed $L_c = 1.1 \times 10^{37} \text{ erg s}^{-1}$ which we inferred from the ‘‘knee’’ seen in the lightcurves of the 1997 and 2010 outbursts in Figure 4.

Our assumption that the rapid decay stage corresponds to the weak propeller regime is not commonly accepted. Given the existence of black hole systems which also show a similar knee in the lightcurve, it may be argued that the rapid decay stage is a property of the disk instability model underlying the outburst (King & Ritter 1998; Campana et al. 2014). According to this picture a cooling front moving inwards in the disc is the cause of the transition to the rapid decay stage. The possibility that the knee seen in the X-ray light curves of outbursting systems is due to the transition to the propeller stage as well as to the disk instability, is argued in the literature (e.g. Gilfanov et al. 1998; Ibragimov & Poutanen 2009; Ekşi & Kutlu 2011; Asai et al. 2013; Güngör et al. 2014). The narrow range of δ values characterizing the transition, as we inferred in this work, supports the view that the rapid decay stage represents transition to the partial accretion regime. The wide range of the f_{min} values may then indicate the varying contribution of sources other than accretion (such as cooling of the star) to the quiescence luminosity. This would im-

ply that that the rapid decay stage in black hole systems has a different cause than neutron star systems such as the truncation of the disk.

6. CONCLUSIONS

Based on our model and the related investigation we conclude that:

- The range $\omega_* \lesssim 0.9$ is the slow decay stage. All of the material transferred from outer disk accretes onto the NS. As \dot{M} ($= \dot{M}_*$ in accretion stage) decreases in time, the luminosity declines (slow decay stage) while R_{in} expands back to R_c .
- The range $0.9 \lesssim \omega_* \lesssim 1.1$ is the partial accretion regime. A fraction of inflowing material to the inner layers of the disk may transfer onto the NS. The rest may be thrown to outer layers of the disk or expelled from the system via jet mechanism.
- The range $\omega_* \gtrsim 1.1$ is the fully developed propeller stage and the neutron star may even act as an isolated NS (Ekşi & Alpar 2005).

ACKNOWLEDGEMENTS

We gratefully acknowledge the anonymous referee for very constructive comments and suggestions. CG thanks The Scientific and Technological Council of TURKEY (TUBITAK) for the 2214-A Scholarship. CG is grateful to Prof. Neuhäuser for 1-year research project in Jena/Germany. CG appreciate Prof. Santangelo for Tübingen visit and useful discussion. KYE, TG and CG acknowledge support from TUBITAK with the project number 112T105. KYE and CG thank İstanbul Technical University Scientific Research Projects Unit (ITU-BAP) for the support with the project number of 38339. This research has made use of the XRT Data Analysis Software (XRTDAS) developed under the responsibility of the ASI Science Data Center (ASDC), Italy.

REFERENCES

- Asai, K., Matsuoka, M., Mihara, T., et al. 2013, *ApJ*, 773, 117
- Balucinska-Church, M., & McCammon, D. 1992, *ApJ*, 400, 699
- Campana, S., Brivio, F., Degenaar, N., et al. 2014, *MNRAS*, 441, 1984
- Campana, S., Coti Zelati, F., & D’Avanzo, P. 2013, *MNRAS*, 432, 1695
- Campana, S., Gastaldello, F., Stella, L., et al. 2001, *ApJ*, 561, 924
- Campana, S., Stella, L., Mereghetti, S., et al. 1998, *ApJL*, 499, L65
- Cannizzo, J. K., Lee, H. M., & Goodman, J. 1990, *ApJ*, 351, 38
- Casella, P., Altamirano, D., Patruno, A., Wijnands, R., & van der Klis, M. 2008, *ApJL*, 674, L41
- Cui, W. 1997, *ApJL*, 482, L163
- D’Angelo, C. R., & Spruit, H. C. 2010, *MNRAS*, 406, 1208
- . 2011, *MNRAS*, 416, 893
- Davidson, K., & Ostriker, J. P. 1973, *ApJ*, 179, 585
- Di Salvo, T., & Burderi, L. 2003, *A&A*, 397, 723
- Ekşi, K. Y., & Alpar, M. A. 2005, *ApJ*, 620, 390
- Ekşi, K. Y., & Kutlu, E. 2011, in *American Institute of Physics Conference Series*, Vol. 1379, American Institute of Physics Conference Series, ed. E. Göğüş, T. Belloni, & Ü. Ertan, 156–159
- Elsner, R. F., & Lamb, F. K. 1977, *ApJ*, 215, 897
- Frank, J., King, A., & Raine, D. J. 2002, *Accretion Power in Astrophysics: Third Edition* (Cambridge University Press)
- Galloway, D. K., Muno, M. P., Hartman, J. M., Psaltis, D., & Chakrabarty, D. 2008, *ApJS*, 179, 360
- Ghosh, P., & Lamb, F. K. 1979a, *ApJ*, 232, 259
- . 1979b, *ApJ*, 234, 296
- Gilfanov, M., Revnivtsev, M., Sunyaev, R., & Churazov, E. 1998, *A&A*, 338, L83
- Güngör, C., Ekşi, K. Y., & Göğüş, E. 2017, *NewA*, 56, 1
- Güngör, C., Güver, T., & Ekşi, K. Y. 2014, *MNRAS*, 439, 2717
- Ibragimov, A., & Poutanen, J. 2009, *MNRAS*, 400, 492
- Illarionov, A. F., & Sunyaev, R. A. 1975, *A&A*, 39, 185
- King, A. L., Tomsick, J. A., Miller, J. M., et al. 2016, *ApJL*, 819, L29
- King, A. R., & Ritter, H. 1998, *MNRAS*, 293, L42
- Koyama, K., Inoue, H., Makishima, K., et al. 1981, *ApJL*, 247, L27
- Lamb, F. K., Pethick, C. J., & Pines, D. 1973, *ApJ*, 184, 271
- Lasota, J.-P. 2001, *NewAR*, 45, 449
- Lin, D., Remillard, R. A., & Homan, J. 2007, *ApJ*, 667, 1073

- Lipunov, V. M., Börner, G., & Wadhwa, R. S. 1992, *Astrophysics of Neutron Stars* (Springer), 108
- Lipunov, V. M., & Shakura, N. I. 1976, *Soviet Astronomy Letters*, 2, 133
- Lipunova, G. V., & Shakura, N. I. 2002, *Astronomy Reports*, 46, 366
- Liu, B. F., Yuan, W., Meyer, F., Meyer-Hofmeister, E., & Xie, G. Z. 1999, *ApJL*, 527, L17
- Lyubarskij, Y. E., & Shakura, N. I. 1987, *Soviet Astronomy Letters*, 13, 386
- Maccarone, T. J., & Coppi, P. S. 2003, *A&A*, 399, 1151
- Maitra, D., & Bailyn, C. D. 2008, *ApJ*, 688, 537
- Menou, K., Esin, A. A., Narayan, R., et al. 1999, *ApJ*, 520, 276
- Meshcheryakov, A. V., Tsygankov, S. S., Khamitov, I. M., et al. 2017, *MNRAS* submitted, arXiv:1703.09159
- Meyer, F., Liu, B. F., & Meyer-Hofmeister, E. 2000, *A&A*, 361, 175
- Mukherjee, D., Bult, P., van der Klis, M., & Bhattacharya, D. 2015, *MNRAS*, 452, 3994
- Özsükan, G., Ekşi, K. Y., Hambaryan, V., et al. 2014, *ApJ*, 796, 46
- Patruno, A., & Watts, A. L. 2012, *ArXiv e-prints*, arXiv:1206.2727
- Pringle, J. E., & Rees, M. J. 1972, *A&A*, 21, 1
- Remillard, R. A., & McClintock, J. E. 2006, *ARA&A*, 44, 49
- Romanova, M. M., & Owocki, S. P. 2015, *SSRv*, 191, 339
- Romanova, M. M., Ustyugova, G. V., Koldoba, A. V., & Lovelace, R. V. E. 2004, *ApJL*, 616, L151
- Sakurai, S., Yamada, S., Torii, S., et al. 2012, *PASJ*, 64, 72
- Shakura, N. I., & Sunyaev, R. A. 1973, *A&A*, 24, 337
- Spruit, H. C., & Taam, R. E. 1993, *ApJ*, 402, 593
- Suleimanov, V. F., Lipunova, G. V., & Shakura, N. I. 2008, *A&A*, 491, 267
- Sunyaev, R. A., & Shakura, N. I. 1977, *Pisma v Astronomicheskii Zhurnal*, 3, 262
- Titarchuk, L. 1994, *ApJ*, 434, 570
- Titarchuk, L., & Lyubarskij, Y. 1995, *ApJ*, 450, 876
- Tsygankov, S. S., Mushtukov, A. A., Suleimanov, V. F., et al. 2017, *A&A* submitted, arXiv:1703.04528
- Tudose, V., Fender, R. P., Linares, M., Maitra, D., & van der Klis, M. 2009, *MNRAS*, 400, 2111
- Ustyugova, G. V., Koldoba, A. V., Romanova, M. M., & Lovelace, R. V. E. 2006, *ApJ*, 646, 304
- Wijnands, R., & van der Klis, M. 1998, *Nature*, 394, 344
- Zhang, S. N., Yu, W., & Zhang, W. 1998a, *ApJL*, 494, L71
- . 1998b, *ApJL*, 494, L71

Table 2. Best fit parameters of *blackbody + disk blackbody + Gauss* model for the 2000 outburst. The horizontal lines in the table indicate the state transitions according to hardness parameter of the blackbody component.

Obs #	ObsID	MJD-51000 (days)	kT_{bbody} (keV)	kT_{diskbb} (keV)	$\chi^2/d.o.f.^a$	Hardness ^b		Flux ^c _{bbody}	Flux ^d _{diskbb}
						bbody	diskbb		
1	50049-01-03-00	811.28564	5.27 ± 1.12	1.19 ± 0.15	0.90	4.36 ± 1.97	1.50 ± 0.06	1.63 ± 0.08	0.60 ± 0.01
2	50049-01-03-01	812.34953	6.96 ± 1.23	1.58 ± 0.10	1.14	6.89 ± 2.81	5.45 ± 0.13	2.70 ± 0.52	1.68 ± 0.02
3	50049-01-03-02	813.27735	6.63 ± 1.40	1.64 ± 0.09	1.00	6.41 ± 1.69	6.43 ± 0.13	4.27 ± 0.49	2.63 ± 0.03
4	50049-01-04-00	816.46667	4.08 ± 0.71	2.10 ± 0.10	1.13	2.64 ± 0.92	14.93 ± 0.20	7.95 ± 1.67	11.29 ± 0.08
5	50049-01-04-01	817.79791	5.88 ± 0.16	2.35 ± 0.05	1.24	5.29 ± 0.36	20.77 ± 0.25	22.94 ± 0.40	18.80 ± 0.11
6	50049-01-04-04	822.77448	2.40 ± 0.08	1.63 ± 0.07	0.69	0.65 ± 0.19	6.23 ± 0.07	27.16 ± 4.01	77.91 ± 0.44
7	50049-01-05-00	823.76888	2.38 ± 0.07	1.71 ± 0.07	0.57	0.64 ± 0.06	7.40 ± 0.14	35.20 ± 0.20	90.30 ± 0.50
8	50049-01-05-01	824.76115	2.28 ± 0.05	1.56 ± 0.08	0.38	0.56 ± 0.11	5.15 ± 0.07	47.76 ± 4.49	72.13 ± 0.48
9	50049-01-05-02	825.75496	2.29 ± 0.08	1.57 ± 0.08	0.63	0.57 ± 0.16	5.31 ± 0.06	31.39 ± 4.32	71.95 ± 0.44
10	50049-02-01-00	826.51291	2.31 ± 0.05	1.64 ± 0.07	0.39	0.59 ± 0.12	6.31 ± 0.07	44.55 ± 4.34	86.14 ± 0.52
11	50049-02-02-00	828.53443	2.34 ± 0.05	1.61 ± 0.05	0.75	0.61 ± 0.12	5.96 ± 0.06	30.32 ± 3.03	79.80 ± 0.45
12	50049-02-03-01	831.20242	2.32 ± 0.07	1.62 ± 0.08	0.49	0.59 ± 0.15	6.12 ± 0.07	37.45 ± 4.64	75.74 ± 0.46
13	50049-02-03-00	833.45856	2.28 ± 0.07	1.57 ± 0.07	0.81	0.57 ± 0.15	5.30 ± 0.06	33.46 ± 4.39	79.95 ± 0.47
14	50049-02-04-00	834.30025	2.31 ± 0.04	1.63 ± 0.06	0.31	0.59 ± 0.09	6.16 ± 0.08	51.16 ± 4.02	87.91 ± 0.55
15	50049-02-03-02	835.19034	2.21 ± 0.06	1.49 ± 0.07	0.40	0.51 ± 0.11	4.33 ± 0.06	28.15 ± 2.96	50.67 ± 0.33
16	50049-02-05-00	835.47605	2.32 ± 0.06	1.65 ± 0.07	0.30	0.59 ± 0.14	6.58 ± 0.07	40.02 ± 4.54	90.68 ± 0.52
17	50049-02-06-00	836.51501	2.35 ± 0.08	1.66 ± 0.08	0.45	0.62 ± 0.18	6.73 ± 0.08	38.97 ± 5.37	92.11 ± 0.52
18	50049-02-06-01	836.59062	2.31 ± 0.08	1.65 ± 0.09	0.61	0.58 ± 0.19	6.47 ± 0.08	44.63 ± 6.76	89.74 ± 0.55
19	50049-02-06-02	836.65903	2.25 ± 0.09	1.58 ± 0.09	0.41	0.54 ± 0.19	5.53 ± 0.07	37.83 ± 6.14	79.84 ± 0.50
20	50049-02-07-00	837.31072	2.30 ± 0.07	1.64 ± 0.09	0.59	0.58 ± 0.16	6.34 ± 0.08	45.08 ± 5.90	86.81 ± 0.54
21	50049-02-07-01	838.58253	2.26 ± 0.08	1.56 ± 0.08	0.78	0.55 ± 0.16	5.21 ± 0.07	35.25 ± 4.99	75.20 ± 0.47
22	50049-02-07-02	839.16547	2.33 ± 0.07	1.66 ± 0.07	0.38	0.60 ± 0.16	6.59 ± 0.08	40.72 ± 5.23	88.67 ± 0.51
23	50049-02-07-03	841.42330	2.29 ± 0.07	1.52 ± 0.08	0.83	0.57 ± 0.14	4.67 ± 0.06	29.26 ± 3.45	63.35 ± 0.40
24	50049-02-07-04	843.42348	2.34 ± 0.08	1.65 ± 0.08	0.47	0.61 ± 0.19	6.52 ± 0.08	35.51 ± 5.09	79.77 ± 0.46
25	50049-02-08-00	844.12055	2.31 ± 0.05	1.62 ± 0.06	0.44	0.58 ± 0.13	6.06 ± 0.07	33.90 ± 3.53	74.70 ± 0.44
26	50049-02-08-01	845.14572	2.25 ± 0.06	1.53 ± 0.09	0.29	0.54 ± 0.11	4.80 ± 0.07	45.79 ± 4.64	64.78 ± 0.45
27	50049-02-08-03	846.20867	2.27 ± 0.07	1.56 ± 0.08	0.47	0.55 ± 0.15	5.20 ± 0.06	30.71 ± 3.89	65.45 ± 0.42
28	50049-02-10-03	849.39406	2.29 ± 0.11	1.57 ± 0.10	0.48	0.57 ± 0.24	5.37 ± 0.06	23.76 ± 4.69	60.09 ± 0.37
29	50049-02-10-02	849.46316	2.36 ± 0.11	1.65 ± 0.09	0.79	0.63 ± 0.26	6.47 ± 0.07	25.65 ± 4.95	68.85 ± 0.40
30	50049-02-10-01	849.53465	2.36 ± 0.11	1.63 ± 0.09	0.89	0.62 ± 0.24	6.26 ± 0.07	26.61 ± 4.62	67.68 ± 0.40
31	50049-02-10-00	850.10229	2.29 ± 0.05	1.61 ± 0.06	0.38	0.57 ± 0.12	5.92 ± 0.07	28.52 ± 2.95	63.79 ± 0.36
32	50049-02-10-05	850.86400	2.25 ± 0.06	1.56 ± 0.08	0.72	0.54 ± 0.14	5.18 ± 0.06	29.09 ± 3.53	56.65 ± 0.36
33	50049-02-11-01	852.58772	2.23 ± 0.11	1.54 ± 0.10	1.13	0.53 ± 0.23	5.01 ± 0.06	24.38 ± 4.74	53.92 ± 0.34
34	50049-02-11-02	852.65313	2.28 ± 0.16	1.60 ± 0.13	0.73	0.56 ± 0.34	5.70 ± 0.07	24.49 ± 5.96	57.21 ± 0.37
35	50049-02-12-01	853.58329	2.21 ± 0.09	1.49 ± 0.09	0.57	0.51 ± 0.15	4.35 ± 0.06	25.43 ± 3.74	48.45 ± 0.33
36	50049-02-12-00	854.27232	2.33 ± 0.06	1.54 ± 0.07	0.76	0.60 ± 0.13	4.90 ± 0.06	18.68 ± 2.09	45.47 ± 0.28
37	50049-02-13-00	855.30361	2.11 ± 0.04	1.18 ± 0.05	0.87	0.45 ± 0.04	1.40 ± 0.02	19.59 ± 0.99	25.38 ± 0.21
38	50049-02-14-00	856.96964	2.25 ± 0.05	1.42 ± 0.07	0.82	0.54 ± 0.10	3.54 ± 0.05	18.73 ± 1.78	34.56 ± 0.24
39	50049-02-15-00	859.24090	2.20 ± 0.05	1.37 ± 0.07	0.99	0.50 ± 0.08	2.97 ± 0.04	15.66 ± 1.44	25.45 ± 0.19
40	50049-02-15-01	860.21521	2.14 ± 0.10	1.41 ± 0.13	0.63	0.46 ± 0.16	3.35 ± 0.05	14.95 ± 2.78	25.42 ± 0.19
41	50049-02-15-08	860.54742	2.10 ± 0.10	1.18 ± 0.08	1.01	0.44 ± 0.10	1.43 ± 0.03	12.74 ± 1.58	15.82 ± 0.15
42	50049-02-15-02	861.11940	2.20 ± 0.06	1.34 ± 0.08	1.12	0.50 ± 0.08	2.71 ± 0.04	11.94 ± 0.89	19.12 ± 0.15
43	50049-02-15-03	861.88606	2.06 ± 0.04	1.12 ± 0.05	0.84	0.41 ± 0.04	1.05 ± 0.02	9.99 ± 0.53	11.14 ± 0.10
44	50049-02-15-04	862.09305	2.11 ± 0.05	1.13 ± 0.05	1.35	0.45 ± 0.05	1.10 ± 0.02	9.18 ± 0.57	10.45 ± 0.10
45	50049-02-15-05	863.23997	2.45 ± 0.08	1.28 ± 0.06	1.72	0.70 ± 0.09	2.13 ± 0.03	5.78 ± 0.39	9.03 ± 0.08
46	50049-02-15-06	864.20819	2.12 ± 0.11	1.16 ± 0.08	0.83	0.45 ± 0.10	1.27 ± 0.03	6.07 ± 0.67	7.24 ± 0.07
47	50049-02-15-07	864.27747	2.24 ± 0.15	1.17 ± 0.08	0.85	0.54 ± 0.14	1.31 ± 0.03	5.46 ± 0.70	7.19 ± 0.08
48	50049-03-01-00	865.27217	4.43 ± 0.34	1.86 ± 0.07	1.48	3.10 ± 0.61	10.09 ± 0.17	3.99 ± 0.17	5.83 ± 0.05
49	50049-03-02-01	866.92250	4.73 ± 0.46	1.74 ± 0.11	0.99	3.53 ± 0.63	7.87 ± 0.25	3.64 ± 0.16	2.63 ± 0.04
50	50049-03-02-00	866.97790	6.05 ± 0.89	1.67 ± 0.17	0.96	5.55 ± 4.06	6.88 ± 0.15	3.55 ± 1.55	2.45 ± 0.03
51	50049-03-03-00	868.23607	6.56 ± 1.37	1.44 ± 0.16	0.74	6.31 ± 4.82	3.75 ± 0.14	2.17 ± 1.49	1.12 ± 0.02
52	50049-03-04-00	869.47435	6.88 ± 1.28	1.32 ± 0.20	0.86	6.78 ± 4.38	2.49 ± 0.11	0.95 ± 0.47	0.38 ± 0.01

^a Degree of freedom (d.o.f) is 48 for all observation.^b Hardness parameters are obtained using the flux ratio of two different energy ranges; $F(10 - 30 \text{ keV})/F(3 - 10 \text{ keV})$. The parameters for diskbb component are multiplied by 10^2 because of low values^c Unabsorbed fluxes of the blackbody components are in units of $10^{-10} \text{ erg s}^{-1} \text{ cm}^{-2}$.^d Unabsorbed fluxes of the disk blackbody components are in units of $10^{-10} \text{ erg s}^{-1} \text{ cm}^{-2}$.

Table 3. Same as Table 2 but for the 2011 outburst.

Obs #	ObsID	MJD-55000	$kT_{bbod\dot{y}}$	kT_{diskbb}	$\chi^2/d.o.f.^a$	Hardness ^b		Flux ^c _{bbod\dot{y}}	Flux ^d _{diskbb}
		(days)	(keV)	(keV)		bbod\dot{y}	diskbb		
1	96440-01-01-00	849.3771	8.04 ± 1.71	1.63 ± 0.07	1.09	8.39 ± 0.32	6.19 ± 0.12	3.74 ± 0.07	2.76 ± 0.03
2	96440-01-01-01	852.4442	12.11 ± 4.58	2.06 ± 0.05	0.98	12.77 ± 0.42	14.08 ± 0.19	6.83 ± 0.11	9.78 ± 0.06
3	96440-01-02-02	855.5727	5.33 ± 0.13	2.45 ± 0.05	1.11	4.45 ± 0.06	23.44 ± 0.26	31.11 ± 0.19	30.63 ± 0.17
4	96440-01-02-00	858.1840	2.24 ± 0.05	1.55 ± 0.06	0.60	0.53 ± 0.01	5.10 ± 0.06	43.52 ± 0.25	91.63 ± 0.54
5	96440-01-02-03	859.6329	2.32 ± 0.05	1.57 ± 0.08	0.54	0.59 ± 0.01	5.36 ± 0.07	74.03 ± 0.41	98.06 ± 0.69
6	96440-01-02-01	861.2549	2.50 ± 0.03	1.69 ± 0.01	1.10	0.74 ± 0.01	3.97 ± 0.20	26.10 ± 0.51	78.60 ± 0.34
7	96440-01-03-02	862.4965	2.24 ± 0.06	1.55 ± 0.07	0.54	0.53 ± 0.01	5.12 ± 0.06	50.02 ± 0.32	102.58 ± 0.63
8	96440-01-03-05	863.3270	2.25 ± 0.07	1.57 ± 0.07	0.71	0.54 ± 0.01	5.32 ± 0.07	52.41 ± 0.35	108.54 ± 0.67
9	96440-01-03-00	864.2559	2.24 ± 0.06	1.57 ± 0.07	0.61	0.53 ± 0.01	5.41 ± 0.07	54.97 ± 0.32	107.14 ± 0.65
10	96440-01-03-03	865.4324	2.34 ± 0.08	1.66 ± 0.06	0.42	0.61 ± 0.01	6.66 ± 0.07	47.21 ± 0.33	119.18 ± 0.65
11	96440-01-03-06	866.2909	2.30 ± 0.08	1.63 ± 0.08	0.52	0.58 ± 0.01	6.14 ± 0.07	56.66 ± 0.40	118.43 ± 0.73
12	96440-01-03-01	867.2569	2.30 ± 0.06	1.64 ± 0.06	0.38	0.58 ± 0.01	6.37 ± 0.07	57.38 ± 0.32	118.24 ± 0.68
13	96440-01-03-04	867.9826	2.32 ± 0.07	1.68 ± 0.07	0.37	0.60 ± 0.01	7.02 ± 0.08	56.88 ± 0.37	125.92 ± 0.74
14	96440-01-04-03	869.2781	2.26 ± 0.07	1.58 ± 0.07	0.53	0.55 ± 0.01	5.44 ± 0.07	51.59 ± 0.35	106.77 ± 0.65
15	96440-01-04-04	871.2958	2.35 ± 0.08	1.69 ± 0.07	0.55	0.61 ± 0.01	7.16 ± 0.08	48.77 ± 0.33	118.72 ± 0.66
16	96440-01-04-01	872.0858	2.22 ± 0.06	1.54 ± 0.07	0.41	0.52 ± 0.01	4.90 ± 0.06	46.96 ± 0.29	93.05 ± 0.57
17	96440-01-04-05	873.0034	2.27 ± 0.04	1.53 ± 0.07	0.49	0.56 ± 0.01	4.78 ± 0.07	80.36 ± 0.41	100.79 ± 0.74
18	96440-01-04-06	875.6732	2.31 ± 0.08	1.65 ± 0.08	0.56	0.59 ± 0.01	6.55 ± 0.07	46.82 ± 0.32	110.27 ± 0.61
19	96440-01-05-00	876.8402	2.27 ± 0.04	1.55 ± 0.08	0.49	0.55 ± 0.01	5.10 ± 0.07	72.06 ± 0.34	91.93 ± 0.64
20	96440-01-05-01	877.4295	2.32 ± 0.07	1.63 ± 0.06	0.59	0.60 ± 0.01	6.21 ± 0.07	44.29 ± 0.29	101.79 ± 0.58
21	96440-01-05-02	877.8880	2.24 ± 0.05	1.54 ± 0.07	0.57	0.53 ± 0.01	5.00 ± 0.06	53.36 ± 0.30	91.42 ± 0.59
22	96440-01-05-03	879.5833	2.24 ± 0.07	1.56 ± 0.07	0.54	0.54 ± 0.01	5.21 ± 0.06	38.17 ± 0.25	82.47 ± 0.49
23	96440-01-05-04	880.6295	2.27 ± 0.08	1.59 ± 0.07	0.70	0.55 ± 0.01	5.67 ± 0.07	38.00 ± 0.26	86.76 ± 0.48
24	96440-01-05-05	882.6413	2.23 ± 0.08	1.56 ± 0.08	0.57	0.53 ± 0.01	5.20 ± 0.07	44.76 ± 0.30	83.84 ± 0.53
25	96440-01-06-00	883.5596	2.27 ± 0.07	1.58 ± 0.07	0.59	0.56 ± 0.01	5.56 ± 0.07	44.31 ± 0.28	84.61 ± 0.51
26	96440-01-06-01	884.6704	2.18 ± 0.05	1.45 ± 0.07	0.88	0.49 ± 0.01	3.79 ± 0.05	35.19 ± 0.21	61.04 ± 0.40
27	96440-01-06-02	885.8371	2.19 ± 0.05	1.44 ± 0.07	0.60	0.50 ± 0.01	3.75 ± 0.05	36.20 ± 0.20	59.89 ± 0.40
28	96440-01-06-03	886.8228	2.22 ± 0.05	1.50 ± 0.08	0.73	0.52 ± 0.01	4.38 ± 0.06	47.34 ± 0.24	65.07 ± 0.42
29	96440-01-06-04	888.2533	2.20 ± 0.06	1.42 ± 0.07	0.65	0.50 ± 0.01	3.48 ± 0.05	29.03 ± 0.17	52.16 ± 0.35
30	96440-01-07-00	890.0729	2.22 ± 0.07	1.44 ± 0.08	0.81	0.52 ± 0.01	3.72 ± 0.05	26.97 ± 0.17	48.77 ± 0.32
31	96440-01-07-01	891.1884	2.26 ± 0.08	1.54 ± 0.08	0.85	0.55 ± 0.01	4.94 ± 0.06	25.15 ± 0.17	54.51 ± 0.32
32	96440-01-07-02	892.2633	2.25 ± 0.09	1.54 ± 0.08	0.41	0.54 ± 0.01	4.99 ± 0.06	24.98 ± 0.17	53.47 ± 0.31
33	96440-01-07-03	893.4686	2.12 ± 0.06	1.40 ± 0.08	0.67	0.45 ± 0.01	3.28 ± 0.05	29.27 ± 0.18	43.78 ± 0.31
34	96440-01-07-04	894.3870	2.15 ± 0.05	1.33 ± 0.07	0.84	0.47 ± 0.01	2.54 ± 0.04	21.01 ± 0.13	32.87 ± 0.23
35	96440-01-07-05	895.2340	2.17 ± 0.06	1.37 ± 0.08	0.72	0.48 ± 0.01	2.95 ± 0.04	21.07 ± 0.13	34.92 ± 0.23
36	96440-01-07-06	896.1426	2.07 ± 0.04	1.29 ± 0.08	0.80	0.41 ± 0.01	2.18 ± 0.04	28.16 ± 0.15	30.50 ± 0.25
37	96440-01-08-00	898.1645	2.06 ± 0.04	1.10 ± 0.04	1.35	0.41 ± 0.01	0.97 ± 0.02	14.75 ± 0.09	17.27 ± 0.15
38	96440-01-08-02	899.0077	2.12 ± 0.06	1.22 ± 0.07	1.54	0.45 ± 0.01	1.65 ± 0.03	15.29 ± 0.11	19.47 ± 0.16
39	96440-01-08-03	900.3845	2.12 ± 0.08	1.20 ± 0.06	1.31	0.45 ± 0.01	1.53 ± 0.03	11.34 ± 0.08	15.41 ± 0.13
40	96440-01-08-04	901.2278	2.10 ± 0.06	1.23 ± 0.07	0.92	0.44 ± 0.01	1.75 ± 0.03	12.26 ± 0.09	15.87 ± 0.12
41	96440-01-08-05	902.0756	2.02 ± 0.05	1.14 ± 0.06	0.78	0.39 ± 0.01	1.15 ± 0.02	11.22 ± 0.08	12.26 ± 0.11
42	96440-01-08-06	903.1209	1.94 ± 0.05	1.03 ± 0.05	0.86	0.34 ± 0.01	0.63 ± 0.01	7.86 ± 0.06	7.10 ± 0.08
43	96440-01-09-00	904.0978	2.29 ± 0.10	1.17 ± 0.06	1.56	0.57 ± 0.01	1.34 ± 0.03	4.44 ± 0.05	5.74 ± 0.05
44	96440-01-09-08	904.3096	2.31 ± 0.10	1.21 ± 0.06	1.35	0.58 ± 0.01	1.63 ± 0.03	3.95 ± 0.04	5.86 ± 0.05
45	96440-01-09-02	906.0508	9.22 ± 3.94	1.81 ± 0.06	0.93	9.85 ± 0.72	9.19 ± 0.17	2.15 ± 0.08	3.47 ± 0.03
46	96440-01-09-03	907.3148	15.80 ± 7.33	1.66 ± 0.05	1.17	15.40 ± 0.96	6.67 ± 0.12	1.56 ± 0.05	1.95 ± 0.02
47	96440-01-09-10	908.0061	7.94 ± 2.18	1.51 ± 0.11	1.03	8.26 ± 0.52	4.63 ± 0.13	2.05 ± 0.06	1.40 ± 0.02
48	96440-01-09-04	908.2906	9.27 ± 2.57	1.49 ± 0.06	1.02	9.92 ± 0.49	4.37 ± 0.09	1.69 ± 0.04	1.22 ± 0.01
49	96440-01-09-05	909.0731	6.65 ± 1.80	1.30 ± 0.09	1.07	6.44 ± 0.27	2.27 ± 0.06	1.56 ± 0.03	0.75 ± 0.01
50	96440-01-09-11	909.2486	7.83 ± 2.14	1.35 ± 0.12	0.84	8.11 ± 0.59	2.78 ± 0.10	1.41 ± 0.05	0.72 ± 0.01
51	96440-01-09-12	910.9905	3.72 ± 3.72	1.11 ± 0.91	0.61	2.09 ± 0.72	0.76 ± 0.27	0.45 ± 0.07	0.16 ± 0.03

^a Degree of freedom (d.o.f) is 49 for all observation.^b Hardness parameters are obtained using the flux ratio of two different energy ranges; $F(10 - 30 \text{ keV})/F(3 - 10 \text{ keV})$. The parameters for disk blackbody component are multiplied by 10^2 because of low values^c Unabsorbed fluxes of the blackbody components are in units of $10^{-10} \text{ erg s}^{-1} \text{ cm}^{-2}$.^d Unabsorbed fluxes of the disk blackbody components are in units of $10^{-10} \text{ erg s}^{-1} \text{ cm}^{-2}$.

Table 4. Best fit parameters of *blackbody + comptonization + disk blackbody + Gauss* model for the 2000 outburst. The horizontal lines in the table indicate the state transitions according to hardness parameter of the blackbody component.

Obs #	kT_{bbody} (keV)	τ	$\chi^2/d.o.f.^a$	Hardness ^b bbody	Flux ^c _{bbody}
1	2.36 ± 0.30	2.72 ± 0.67	0.95	2.77 ± 0.10	1.84 ± 0.02
2	2.80 ± 0.21	2.49 ± 0.30	1.13	3.30 ± 0.09	3.37 ± 0.03
3	2.77 ± 0.21	2.76 ± 0.26	1.03	3.49 ± 0.08	5.10 ± 0.04
4	3.61 ± 0.36	2.38 ± 0.60	0.68	4.73 ± 0.07	16.74 ± 0.07
5	3.44 ± 0.70	2.44 ± 0.16	0.69	4.31 ± 0.06	24.74 ± 0.10
6	2.17 ± 0.13	0.12 ± 0.04	0.63	0.59 ± 0.01	30.91 ± 0.17
7	2.34 ± 0.05	0.01 ± 0.01	0.62	0.65 ± 0.01	34.82 ± 0.20
8	2.24 ± 0.03	0.10 ± 0.02	0.32	0.56 ± 0.01	48.09 ± 0.21
9	2.22 ± 0.05	0.01 ± 0.01	0.68	0.60 ± 0.01	30.65 ± 0.17
10	2.27 ± 0.03	0.01 ± 0.01	0.51	0.60 ± 0.01	44.13 ± 0.20
16	2.25 ± 0.03	0.13 ± 0.09	0.52	0.58 ± 0.01	40.97 ± 0.20
31	2.25 ± 0.04	0.11 ± 0.10	0.49	0.56 ± 0.01	28.96 ± 0.14
39	2.00 ± 0.03	0.06 ± 0.02	0.93	0.48 ± 0.01	16.36 ± 0.07
41	1.91 ± 0.03	0.03 ± 0.02	1.30	0.40 ± 0.01	13.82 ± 0.07
44	1.70 ± 0.06	0.45 ± 0.36	1.74	0.34 ± 0.01	12.04 ± 0.05
45	1.80 ± 0.08	0.48 ± 0.13	1.99	0.49 ± 0.01	7.85 ± 0.03
46	1.95 ± 0.04	0.01 ± 0.01	1.63	0.40 ± 0.01	6.74 ± 0.04
47	2.01 ± 0.15	0.11 ± 0.07	0.80	0.53 ± 0.01	5.65 ± 0.04
48	3.48 ± 0.45	1.63 ± 0.51	1.40	3.27 ± 0.13	4.06 ± 0.05
49	3.75 ± 0.65	2.30 ± 0.88	0.93	3.71 ± 0.19	3.71 ± 0.07
50	2.82 ± 0.40	2.83 ± 0.22	0.91	3.64 ± 0.11	4.00 ± 0.04
51	2.72 ± 0.48	2.84 ± 0.85	0.67	3.47 ± 0.15	2.49 ± 0.04
52	2.55 ± 0.56	2.98 ± 0.20	0.78	3.29 ± 0.15	1.07 ± 0.02

^a Degree of freedom (d.o.f) is 49 for all observation.^b Hardness parameters are obtained using the flux ratio of two different energy ranges; $F(10 - 30 \text{ keV})/F(3 - 10 \text{ keV})$.^c Unabsorbed fluxes of the blackbody components are in units of $10^{-10} \text{ erg s}^{-1} \text{ cm}^{-2}$.

Table 5. Same as [Table 4](#) but for the 2011 outburst.

Obs #	kT_{bbody} (keV)	τ	$\chi^2/d.o.f.^a$	Hardness ^b bbody	Flux ^c _{bbody}
1	2.83 ± 0.31	2.57 ± 0.45	1.18	3.36 ± 0.07	5.27 ± 0.04
2	3.82 ± 0.40	2.16 ± 0.77	1.08	4.94 ± 0.13	13.76 ± 0.10
3	2.98 ± 0.58	1.91 ± 0.85	0.96	3.07 ± 0.05	37.48 ± 0.19
4	2.21 ± 0.04	0.01 ± 0.01	0.67	0.54 ± 0.01	43.37 ± 0.21
5	2.29 ± 0.03	0.01 ± 0.01	0.66	0.60 ± 0.01	73.84 ± 0.30
6	2.47 ± 0.01	0.01 ± 0.01	1.79	0.71 ± 0.01	26.81 ± 0.17
7	2.17 ± 0.04	0.01 ± 0.01	0.72	0.54 ± 0.01	49.46 ± 0.26
8	2.18 ± 0.04	0.07 ± 0.05	0.92	0.53 ± 0.01	53.56 ± 0.28
9	2.19 ± 0.03	0.09 ± 0.08	0.74	0.52 ± 0.01	55.90 ± 0.27
10	2.28 ± 0.05	0.21 ± 0.21	0.52	0.59 ± 0.01	48.14 ± 0.27
12	2.25 ± 0.03	0.01 ± 0.01	0.60	0.59 ± 0.01	56.81 ± 0.28
19	2.21 ± 0.03	0.06 ± 0.04	0.86	0.54 ± 0.01	73.73 ± 0.28
30	2.06 ± 0.05	0.07 ± 0.03	0.75	0.51 ± 0.01	27.71 ± 0.14
40	1.83 ± 0.10	0.34 ± 0.23	0.95	0.37 ± 0.00	14.42 ± 0.07
41	1.84 ± 0.02	0.04 ± 0.02	1.09	0.37 ± 0.01	11.89 ± 0.06
42	1.67 ± 0.05	0.10 ± 0.01	0.91	0.30 ± 0.00	8.92 ± 0.04
43	1.80 ± 0.01	0.40 ± 0.03	1.35	0.45 ± 0.01	5.52 ± 0.03
44	1.64 ± 0.04	0.34 ± 0.03	1.76	0.41 ± 0.01	5.50 ± 0.03
45	3.60 ± 0.60	2.66 ± 0.60	0.91	3.67 ± 0.12	3.64 ± 0.04
46	3.17 ± 0.47	3.15 ± 0.48	1.32	3.55 ± 0.04	3.06 ± 0.02
47	2.51 ± 0.24	3.00 ± 3.00	1.07	2.89 ± 0.09	2.73 ± 0.03
48	2.70 ± 0.30	2.68 ± 0.17	1.17	3.28 ± 0.08	2.40 ± 0.02
49	2.14 ± 0.16	2.99 ± 0.05	1.24	2.54 ± 0.06	1.91 ± 0.02
50	2.39 ± 0.25	3.01 ± 0.08	0.84	2.75 ± 0.09	1.77 ± 0.02
51	3.24 ± 1.59	2.74 ± 2.61	0.56	1.82 ± 0.44	0.47 ± 0.06

^a Degree of freedom (d.o.f) is 50 for all observation.^b Hardness parameters are obtained using the flux ratio of two different energy ranges; $F(10 - 30 \text{ keV})/F(3 - 10 \text{ keV})$.^c Unabsorbed fluxes of the blackbody components are in units of $10^{-10} \text{ erg s}^{-1} \text{ cm}^{-2}$.